THE JOURNAL OF BIOLOGICAL CHEMISTRY VOL. 287, NO. 35, pp. 29290–29300, August 24, 2012

Protein Disulfide Isomerase Is Required for Platelet-derived Growth Factor-induced Vascular Smooth Muscle Cell Migration, Nox1 NADPH Oxidase Expression, and RhoGTPase Activation[S]

Received for publication, June 21, 2012 Published, JBC Papers in Press, July 6, 2012, DOI 10.1074/jbc.M112.394551

Luciana A. Pescatore[‡], Diego Bonatto[§], Fábio L. Forti[¶], Amine Sadok[‖], Hervé Kovacic[‖], and Francisco R. M. Laurindo[‡1]

From the [‡]Vascular Biology Laboratory, Heart Institute (InCor), University of São Paulo School of Medicine, São Paulo, Brazil 05403-000, the [§]Biotechnology Center, Molecular Biology and Biotechnology Department, Federal University of Rio Grande do Sul, Porto Alegre, Rio Grande do Sul, Brazil 91509-900, the [¶]Chemistry Institute, University of São Paulo, São Paulo, Brazil 05508-000, and [‖]1-Aix-Marseille University, CRO2-INSERM UMR 911, 13385 Marseille, France

Background: Protein disulfide isomerase (PDI) regulates Nox NADPH oxidase activity.
Results: PDI silencing promoted decreased platelet-derived growth factor-induced reactive oxygen species, Nox1 expression, and cell migration. Mechanism involves disruptions of: Rac1/RhoA activation, cytoskeletal organization, and PDI/RhoGDI interaction.
Conclusion: PDI is required for redox-mediated vascular smooth muscle migration.
Significance: ER redox chaperone PDI adds a novel regulatory level to redox/GTPase-related cell migration.

Vascular Smooth Muscle Cell (VSMC) migration into vessel neointima is a therapeutic target for atherosclerosis and postinjury restenosis. Nox1 NADPH oxidase-derived oxidants synergize with growth factors to support VSMC migration. We previously described the interaction between NADPH oxidases and the endoplasmic reticulum redox chaperone protein disulfide isomerase (PDI) in many cell types. However, physiological implications, as well as mechanisms of such association, are yet unclear. We show here that platelet-derived growth factor (PDGF) promoted subcellular redistribution of PDI concomitant to Nox1-dependent reactive oxygen species production and that siRNA-mediated PDI silencing inhibited such reactive oxygen species production, while nearly totally suppressing the increase in Nox1 expression, with no change in Nox4. Furthermore, PDI silencing inhibited PDGF-induced VSMC migration assessed by distinct methods, whereas PDI overexpression increased spontaneous basal VSMC migration. To address possible mechanisms of PDI effects, we searched for PDI interactome by systems biology analysis of physical protein-protein interaction networks, which indicated convergence with small GTPases and their regulator RhoGDI. PDI silencing decreased PDGF-induced Rac1 and RhoA activities, without changing their expression. PDI co-immunoprecipitated with RhoGDI at base line, whereas such association was decreased after PDGF. Also, PDI co-immunoprecipitated with Rac1 and RhoA in a PDGF-independent way and displayed detectable spots of perinuclear co-localization with Rac1 and RhoGDI. Moreover, PDI silencing promoted strong cytoskeletal changes: disorganization of stress fibers, decreased number of focal adhesions, and reduced number of RhoGDI-containing vesicular recycling adhesion structures. Overall, these data suggest that PDI is required to support Nox1/redox and GTPase-dependent VSMC migration.

Vascular smooth muscle cell (VSMC)[2] migration is a crucial mechanism and powerful therapeutic target in the genesis of most vascular diseases, including atherosclerosis and restenosis after angioplasty (1). Redox processes are important mediators of growth factor-induced VSMC migration. Several studies showed that general inhibitors of reactive oxygen species (ROS) promote decrease in platelet-derived growth factor (PDGF)-induced migration (2, 3) by mechanisms downstream of PDGF binding to its receptor (3). Nox family NADPH oxidases, a major dedicated source of signaling ROS in most cells, closely synergize with growth factor-mediated signals to support VSMC migration. Silencing of Nox1 isoform inhibits ROS generation, migration, and metalloproteinase secretion in FGF-stimulated VSMCs (4). Also, VSMCs from Nox1 y/− mice show impaired migration in response to thrombin (5), as well as FGF, the latter recovered by retroviral Nox1 restitution (4). VSMC migration is also influenced by Nox4 via mechanisms involving its novel regulator Poldip2 (6), which fine-tunes the optimal level of focal adhesion turnover. However, pathways that adjust Nox activation to specific physiologic programs in cells are unclear. Our group has provided evidence that the

[S] This article contains supplemental Tables S1–S4, Figs. S1–S4, Methods, Results, and additional references.

[1] To whom correspondence should be addressed: Heart Institute (InCor), University of São Paulo School of Medicine, Vascular Biology Laboratory, Av. Eneas Carvalho Aguiar, 44, Annex II, 9th floor, CEP 05403-000, São Paulo, Brazil. Tel.: 55-11-26615968; Fax: 55-11-26615920; E-mail: francisco.laurindo@incor.usp.br.

[2] The abbreviations used are: VSMC, vascular smooth muscle cell; AngII, angiotensin II; DHE, dihydroethidium; DTPA, diethylentriamene pentaacetate; EOH, 2-hydroxyethidium; ER, endoplasmic reticulum; PDI, protein disulfide isomerase; PPPI, physical protein-protein interaction; ROS, reactive oxygen species.

endoplasmic reticulum (ER) redox chaperone protein disulfide isomerase (PDI) functionally regulates NADPH oxidase and associates with its subunits in distinct cell types (7–10). PDI is the founding member of a large protein family belonging to the thioredoxin superfamily of dithiol-disulfide oxidoreductases, displaying thiol isomerase, oxidase, and reductase activities (11–14). The canonical function of PDI is to assist in disulfide bond introduction and protein folding in the ER lumen (15). Other effects in subcellular traffic and protein secretion (16), mRNA translation (17), antigen presentation (18, 19), as well as several effects at cell surface location (20–22) have also been described. Antagonism or silencing of PDI markedly prevents angiotensin II (AngII)-induced ROS production, NADPH oxidase activity, Nox1 mRNA expression, and Akt phosphorylation (8, 10) in VSMCs. Contrarily, induced PDI overexpression promotes preemptive spontaneous ROS generation, NADPH oxidase activity, and Nox1, but not Nox4 mRNA expression (8). In J-774 macrophages, PDI overexpression increases, whereas PDI silencing decreases *Leishmania chagasi* phagocytosis and NADPH oxidase activation (9). Moreover, we recently showed PDI requirement for activation of neutrophil NADPH oxidase, in both cell-free and whole cell systems (7). In all such cell types, PDI co-localizes and/or co-immunoprecipitates with several catalytic or regulatory ($p22^{phox}$ or $p47^{phox}$) oxidase subunits (7, 9, 10). Overall, the versatile functions of PDI in central housekeeping processes such as protein folding and in other cellular signaling programs indicate that PDI(s) is(are) strategic to integrate cell homeostasis and signaling via pathways that include Nox-related redox processes. However, despite substantial evidence for links between PDI and NADPH oxidase activity, there is less evidence for physiological implications of this interaction. Moreover, mechanisms whereby PDI converges with Nox complex(es) are unclear. In the present study, we addressed the effect of PDI in PDGF-induced VSMC migration, which is associated with NADPH oxidase activation and ROS-dependent signaling. Moreover, using system biology tools to examine protein-protein interaction, as well as experimental approaches, we identified and provided evidence for a role of RhoGTPases and their regulator RhoGDI as possible mechanistical targets underlying the interplay between PDI and Nox-dependent VSMC migration.

EXPERIMENTAL PROCEDURES

Cell Culture and Transfection—Rabbit aortic VSMCs from a previously established selection-immortalized line were maintained in growth medium (F12, with 10% fetal bovine serum) at 37 °C, in 5% CO_2 atmosphere. For transfection, VSMCs were plated at 40% (small interfering RNA) or 60% (plasmid) confluence on 6-well plates. After 8–12 h, cells were serum-starved for 12–16 h before transfection. Lipofectamine 2000 (3 μl; Invitrogen) alone or with Stealth® siRNA (50 nM; Invitrogen) or its scrambled nontargeting control siRNA (ScrRNA) transfection was performed in growth medium without serum and antibiotics for 6 h. Three different siRNA sequences against PDI were used: (#1 primer, 5′-G A G G U G G C C U U U G A C G A G A A G A A G A-3′; #2 primer, 5′-C A A G C A C C U G C U G G U G G A G U U C U A U-3′; #3 primer, 5′-G A C G A C A U U G U G A A C U G G C U G A A G A-3′;). The siRNA sequence against Nox1 was 5′-A C G A U A G C C U U G A U U C U C A U G G U A A-3′. Transient transfection with cDNA plasmids was performed with Lipofectamine 2000 (5 μl) and 5 μg of human PDI cDNA (kindly provided by Drs. Mariano Janiszewski and Lucia Lopes, from the University of São Paulo Biomedical Institute) or pCDNA3 (empty vector control) for 8 h. After siRNA or cDNA transfection, medium was replaced by growth medium for 72 h (siRNA) or 48 h (cDNA). Cultures were serum-starved for 12–24 h prior to treatment with human recombinant platelet-derived growth factor-BB (PDGF; Sigma).

Detection of ROS Production in Whole VSMCs—ROS production in whole VSMCs was assessed by HPLC analysis of dihydroethidium (DHE)-derived oxidation products, as described (23, 24), in duplicate or triplicate experiments. Results are expressed for 2-hydroxyethidium (EOH), which is specific for superoxide, and ethidium, which reflects less specific oxidants. Briefly, at base line or after previous stimulus, VSMCs were incubated for 30 min with 80 μM DHE on Krebs/0.1 mM DTPA. Cells were harvested in acetonitrile and centrifuged (12,000 × *g* for 10 min at 4 °C). The homogenate was dried under vacuum and analyzed by HPLC with fluorescence detectors (Waters). Quantification of DHE, EOH, and ethidium concentrations was performed as described (23, 24), by comparison of integrated peak areas between the obtained and standard curves of each product under identical chromatographic conditions. EOH and ethidium were monitored by fluorescence detection with excitation 480 nm and emission 580 nm (23), whereas DHE was monitored by ultraviolet absorption at 245 nm. Results were expressed as calculated EOH or ethidium concentrations (micromolar), normalized for consumed DHE (*i.e.* initial minus remaining DHE concentration in the sample).

DHE-derived NADPH Oxidase Assay—VSMCs were incubated or not with PDGF (100 ng/ml for 2 h), and membrane homogenates were obtained by sequential centrifugation (23). The assay was performed as described (24), through incubation of NADPH substrate with membrane fraction and assessment of superoxide product. Briefly, VSMCs were disrupted by sonication in buffer containing 50 mM Tris, pH 7.4, 0.1 mM EDTA, 0.1 mM EGTA, and protease inhibitors (10 mg/ml aprotinin, 10 mg/ml leupeptin, and 1 mM PMSF) and centrifuged (18,000 × *g*, 15 min). After supernatant centrifugation (100,000 × *g*, 1 h), the membrane pellet was resuspended in the same buffer. Membrane fraction (40 μg of protein) was incubated with 80 μM DHE in Tris buffer (50 mM, pH 7.4) with DTPA 0.1 mM in the presence of NADPH (300 μM) for 30 min at 37 °C in the dark. After precipitation with trichloroacetic acid, the membrane fraction underwent another centrifugation (12,000 × *g*, 10 min). The final supernatant was analyzed by HPLC/fluorescence detection (excitation 480 nm/emission 580 nm) (23), whereas DHE was monitored by ultraviolet absorption at 245 nm. Specificity for superoxide detection by this assay in Fig. 1*D* was tested with CuZnSOD incubation (25 μg/ml).

Cell Migration Assays—The Transwell assay (Boyden Chamber) was modified from a previous report (3). Briefly, 5×10^4 cells/well, previously starved (~16 h), were added to the upper well, over a polycarbonate membrane (8 μm; Whatman). In

some experiments, diphenyleneiodonium was added to the culture medium with the cells. PDGF (at described concentrations) was used as chemotactic stimulus at the lower well. After 4 h at 37 °C, nonmigrating cells were removed with a cotton swab, and the migrating cells at the membrane bottom side were stained with DAPI (1:100). Four fields/well were used to count the number of migrating cells on inverted microscope (Axiovert 200; Zeiss). Every condition was tested at least on duplicate wells. The wound-healing model was performed as described previously (25). Briefly, monolayer VSMCs cultured in 12-well plates were starved for 24 h. The pictures were taken from the monolayer scratch before and 16 h after PDGF stimulus. Cell migration was evaluated at these two time points with ImageJ software. Data were expressed as the percentage of recovered surface on PDGF-induced cells minus base line condition. Every condition was performed at least in duplicate, and at least 10 pictures were taken on inverted microscope (Axiovert 200).

Quantitative PCR—Nox1 and Nox4 mRNA quantification were performed as described (26). Isolated RNA (RNA Spin Mini kit; GE Healthcare) was reverse-transcribed with Superscript II (Invitrogen). Message expression was quantified with the use of SYBR Green PCR Mix and the Rotorgene 6000 cycler (Corbett) with Master Mix (Invitrogen) and Nox1 or Nox4 primers normalized to GADPH housekeeping. Forward primers, designed according to rabbit sequences, were: Nox1, C A T C A T G G A A G G A A G G A G A; Nox4, C C A C A G A C T T G G C T T T G G A T; GAPDH, T C A C C A T C T T C C A G G A G C G A. The incubation conditions were: 95 °C for 10 min, followed by 40 cycles of 15 s at 94 °C, annealing for 15 s, at 60 °C, and extension for 20 s at 72 °C.

Pulldown Assay of Activated RhoA and Rac1—Assessment of Rac1 or RhoA activities was performed as described (27). VSMCs were harvested on lysis buffer (50 mM Tris, pH 7.2, 500 mM NaCl, 10 mM $MgCl_2$, 1% Triton X-100, 0.1% SDS, 0.5% sodium deoxycholate containing protease and phosphatase inhibitors) and centrifuged at 13,000 × *g*, 10 min, 4 °C. Homogenates (500 μg) were incubated for 90 min at 4 °C with 20 μg of glutathione *S*-transferase-Pak1 binding domain (GST-PBD, to detect active Rac1) or with glutathione *S*-transferase-Rhotekin binding domain (GST-RBD, to detect active RhoA), previously coupled to glutathione-Sepharose. After washing four times (50 mM Tris, pH 7.5, 0.5% Triton X-100, 150 mM NaCl, 5 mM $MgCl_2$), proteins retained on the resins were analyzed by immunoblotting with anti-Rac1 or anti-RhoA antibody.

Western Blot Analysis—Equal amounts of protein from lysates were resolved SDS-PAGE. Primary antibodies were mouse anti-PDIA1 (Enzo Life Science, catalog no. SPA891, 1:1000), mouse anti-Rac1 (Abcam, catalog no. ab33186, 1;1000), mouse anti-RhoA (Santa Cruz Biotechnology, catalog no. SC26C4, 1:1000), rabbit anti-RhoGDI (Abcam, catalog no. ab53850, 1:1000) or mouse anti-β-actin (Sigma, catalog no. A5441, 1:10,000). After incubation with appropriate peroxidase-conjugated secondary antibodies, proteins were visualized by an enhanced chemiluminescence detection kit (Amersham Biosciences).

Confocal Immunofluorescence Experiments—VSMCs were seeded onto glass coverslips for 24 h before PDGF stimulus. Cells were fixed in 4% paraformaldehyde (1 h), permeabilized in 0.1% Nonidet p40 (30 min), and blocked with 2% bovine serum albumin (30 min). Primary antibodies, incubated overnight at 4 °C, were: mouse anti-PDIA1 (Enzo Life Science, 1:200), rabbit anti-PDIA1 (Enzo Life Science, catalog no. SPA890, 1:150), mouse anti-Rac1 (Abcam, 1:50), rabbit anti-RhoGDI (Abcam, 1:50), and rabbit anti-paxillin (Abcam, catalog no. ab32084). Fluorescent secondary antibodies, incubated for 1 h, 25 °C, were Alexa Fluor 488 (rabbit, 1:300) or 546 (mouse, 1:200). F-actin was stained with Alexa Fluor 635 phalloidin (catalog no. A34054, 1:100; Invitrogen). Nuclei were stained with DAPI (Invitrogen, 1:200). Cells were observed under oil immersion 63× objective on an inverted laser confocal microscope (Zeiss LSM510-Meta) at the Confocal "Rede Premium" Multiuser Facility from our institution. Pinhole was adjusted according to objective and sample thickness. Co-localization images represent one slice of 0.5 μm and not the sum of slices. Every condition was assessed from experiments performed in duplicate, and at least 10 images were collected for each coverslip. Results reflect images from at least three independent experiments.

Co-immunoprecipitation Experiments—VSMCs were lysed with 50 mM Tris lysis buffer containing 1% Triton X-100. Immunoprecipitation was performed with 1 mg of lysate using specific antibodies against PDI (10 μg of mouse anti-PDIA1; Enzo Life Science), or anti-Rac1 (5 μg; Abcam), overnight at 4 °C. Protein G-Sepharose bead was added for 2 h, 4 °C. After washing five times, proteins retained on the resins were analyzed by immunoblotting with specific antibodies.

Physical Protein-Protein Interaction (PPPI) Network Design and Global Topological Analysis—The interactomic data gathered from human PDI proteins were used to obtain information about their potential interactions with other proteins in the context of physical protein-protein interactions (PPPI networks) in *Homo sapiens.* In this sense, the data mining screening and network design of a major PPPI network were performed using Cytoscape software, version 2.6.3 (28). For this purpose, we used the PPPI data of *H. sapiens* available in the STRING 9 data base. The PDI-associated PPPI networks obtained from this first screening were then combined in a unique PPPI network by employing the union function of the Cytoscape core plugin Merge Networks. The major PPPI network was then analyzed with Molecular Complex Detection (MCODE) software (29) to detect subnetworks or cluster of proteins that could represent distinct biologic processes.

Network Centralities and Gene Ontology Analyses—Network centralities (bottleneck nodes) were evaluated by using the Cytoscape plugin Cyto-Hubba (30). Gene Ontology clustering analysis was performed using Biological Network Gene Ontology (BiNGO) (31) software, a Cytoscape plugin. The degree of functional enrichment for a given cluster and category was quantitatively assessed (*p* value) by hypergeometric distribution (32), and a multiple test correction was applied using the false discovery rate (33) algorithm, fully implemented in BiNGO software. Overrepresented biological process categories were generated after false discovery rate correction, with a significance level of 0.05.

Statistical Analysis—Values are expressed as mean ± S.D. Statistical comparisons were performed with Student's *t* test for

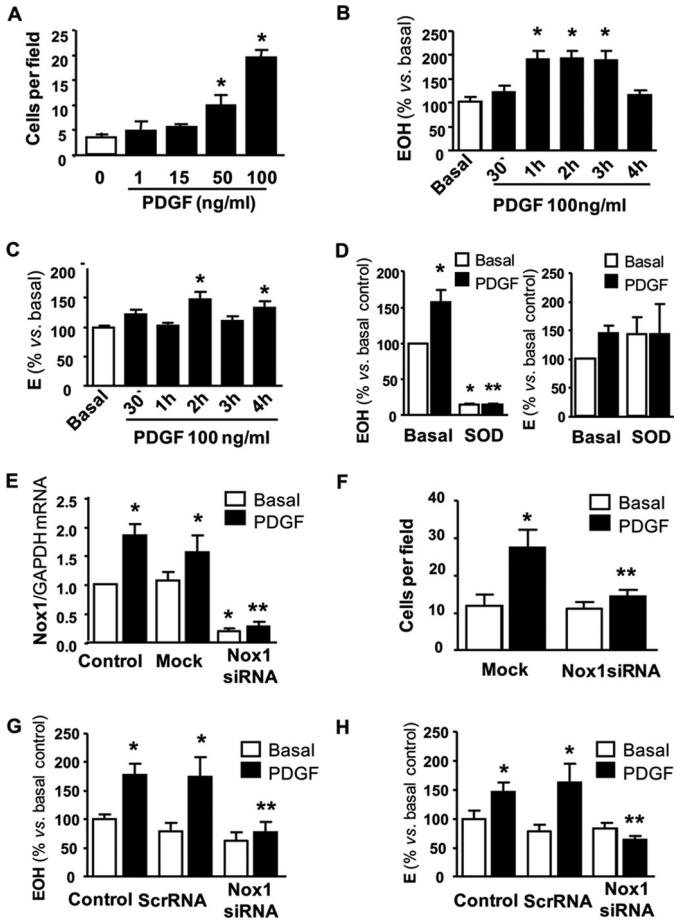

FIGURE 1. **PDGF effects on ROS generation, NADPH oxidase activity, Nox1 isoform expression, and VSMC migration.** *A*, PDGF dose-response curve for VSMC migration in Boyden chamber. *B*, time course of PDGF effect on superoxide production, assessed by HPLC analysis of DHE oxidation through EOH signal. *C*, similar to *B*, with respect to ethidium (*E*) product; *D*, NADPH oxidase activity assay in VSMC membrane fraction incubated with exogenous NADPH at base line or after PDGF stimulus (100 ng/ml, 2 h) and effects of CuZnSOD incubation (25 μg/ml). EOH and ethidium signals were detected through HPLC analysis with fluorescence detection, as described under "Experimental Procedures." *E*, quantitative PCR analysis depicting effects of siRNA silencing on Nox1 mRNA levels at base line or after PDGF incubation (100 ng/ml; 4 h). *F*, effects of Nox1 silencing on VSMC migration, assessed through Boyden chamber assay, at base line and after PDGF (100 ng/ml; 4 h). *G*, effects of Nox1 silencing on whole cell superoxide production measured by HPLC analysis of EOH product at base line or after PDGF (100 ng/ml; 2 h). *H*, similar to *G*, with respect to ethidium product. *Control*, intact VSMC without transfection; *Mock*, VSMC exposed to transfection reagent (Lipofectamine 2000); *ScrRNA*, VSMC transfected with scrambled sequence of siRNA; *Nox1siRNA*, VSMC transfected with siRNA against Nox1. Data are mean ± S.D. (*error bars*) of 3–6 independent experiments per group. *, $p < 0.05$ *versus* basal control; **, $p < 0.05$ *versus* control with PDGF.

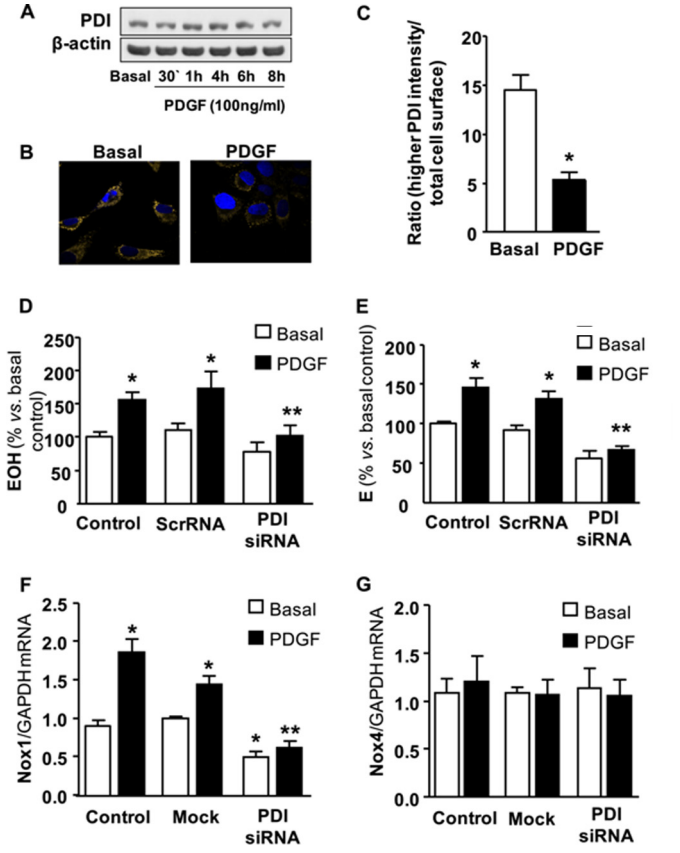

FIGURE 2. **Effects of PDI silencing via siRNA on PDGF-induced ROS production and Nox isoform expression in VSMC.** *A*, Western blot analysis depicting total PDI expression at distinct times after PDGF incubation. *B*, PDI subcellular distribution in VSMCs by confocal microscopy analysis in the absence (*left*) or presence (*right*) of PDGF stimulus. *C*, quantitative analysis of perinuclear PDI fluorescence in conditions similar to *A*, using morphometrys software (QWin). *D*, total superoxide production measured by HPLC analysis of EOH product at base line or after PDGF (100 ng/ml; 2 h). *E*, HPLC analysis of ethidium (*E*) product in conditions similar to *D*. *F*, quantitative PCR analysis depicting mRNA levels of Nox1 at base line or after PDGF incubation (100 ng/ml; 4 h). *G*, analysis of Nox4 mRNA in conditions similar to *F*. *Control*, intact VSMC without transfection; *Mock*, VSMC exposed to transfection reagent (Lipofectamine 2000); *ScrRNA*, VSMC transfected with scrambled sequence of siRNA; *PDI siRNA*, VSMC transfected with siRNA against PDI. Data are mean ± S.D. (*error bars*) of 3–6 independent experiments per group. *, $p < 0.05$ *versus* basal control; **, $p < 0.05$ *versus* control with PDGF.

unpaired data or one-way ANOVA, followed by Student-Newman-Keuls multiple-range test, at 0.05 significance level, using GraphPad Prism v.5 software.

RESULTS

PDGF Increases ROS Generation and Nox1 Expression—Previous reports showed that Nox1-derived ROS production is involved in signaling associated with VSMC migration (3, 4). We first characterized the migratory ROS-dependent effect of PDGF in our cells by a dose-effect curve on the chemotaxis migration assay (Boyden chamber; Fig. 1*A*). As shown in Fig. 1, *B* and *C*, PDGF induced an increase in total production of superoxide (followed by EOH signal at 1, 2, and 3 h) and other oxidants (as seen by the ethidium (*E*) signal at 2 and 4 h). Such an increase in ROS generation after PDGF (2 h) was accompanied by enhanced NADPH oxidase activity in the VSMC membrane fraction (Fig. 1*D*). PDGF-induced migration and ROS production were nearly completely inhibited by the flavoenzyme inhibitor diphenyleneiodonium (supplemental Fig. S1, *A* and *B*). Moreover, silencing of Nox1 NADPH oxidase isoform, confirmed by mRNA level measurements (Fig. 1*E*), also led to an essentially complete inhibition of PDGF-induced VSMC migration (Fig. 1*F*) as well as generation of superoxide (Fig. 1*G*) and ethidium-triggering oxidants (Fig. 1*H*).

PDGF Induces PDI Subcellular Redistribution—We further assessed the behavior of PDI regarding localization and expression in response to PDGF pro-migratory stimulus. Despite no change in total PDI expression after PDGF incubation for 30 min and 1, 4, 6, or 8 h (Fig. 2*A*), analysis of subcellular distribution pattern of PDI by confocal fluorescence microscopy indi-

cated significant changes in PDI redistribution. At base line, PDI showed strong staining at the perinuclear region, whereas after PDGF stimulus, PDI staining around the perinuclear area decreased and showed more diffuse staining scattered throughout the cell (Fig. 2*B*). This is evident by quantification of the most intense fluorescent pixels by a Morph analysis software (software QWin) (Fig. 2*C*). This fluorescence shift may result from changes in cell morphology as well as redistribution of PDI after PDGF similar to that observed with AngII, in which PDI translocates from the soluble to the particulate fraction of VSMC homogenates (10).

PDI Silencing Decreases Nox1 Expression and ROS Production—We previously showed that PDI silencing in VSMC prevented AngII-induced increase in Nox1 mRNA and ROS production (8, 10). We investigated the effects of siRNA-induced PDI silencing on ROS generation and Nox expression induced by PDGF. PDGF-dependent increases in total ROS production (Fig. 2, *D* and *E*) and Nox1 mRNA expression (Fig. 2*F*) were essentially abrogated after PDI siRNA. Under these conditions, there was no significant change in Nox4 mRNA level (Fig. 2*G*). PDI siRNA did not affect the PDGF-induced increase in ERK phosphorylation (data not shown), suggesting that PDI silencing did not promote a nonspecific disruption of signaling downstream from the PDGF receptor.

PDI Is Required for VSMC Migration—The chemotaxis migration assay (Boyden chamber) showed significant decrease in PDGF-induced VSMC migration after PDI silencing with two different siRNA sequences (Fig. 3, *A* and *B*) compared with mock control. Additional experiments showed that such mock control was similar to control cells without transfection at base line or after PDGF (data not shown). Further experiments using the wound-healing assay similarly showed highly significant decreases in PDGF-dependent recovered surface (Fig. 3*C*). Single-cell migration analysis (data not shown) also showed that PDI silencing completely blocked directional persistence of migration. These results indicate the requirement for PDI to support PDGF-induced VSMC migration. PDI gain of function was also tested. PDI overexpression (~2×) increased base-line VSMC migration by an average of 35% compared with empty vector VSMC transfection (Fig. 3*D*), while inducing no further change in PDGF-enhanced migration (Fig. 3*E*).

PPPI Networks Indicate Convergence between PDI and RhoGTPases—The above results indicated a functional effect of PDI on VSMC migration, ROS production, Nox1 expression, and NADPH oxidase activation. To gain insights into possible mechanisms underlying these effects, we performed unbiased searches for proteins interacting with PDI by means of systems biology methods analyzing PPPI networks, an increasingly emerging method to allow hypothesis formulation (34). PPPI networks using human data were retrieved from STRING data base (supplemental Methods and Results). Data were collected for either PDIA1 or PDIA2, given their similarity of structure and function, differing mainly in tissue location (35). Shared proteins and subnetworks from the major PPPI network were identified (supplemental Fig. S2) and retrieved using the Cytoscape-associated plugin MCODE and subjected to a Gene Ontology analysis (supplemental Methods and Results and Tables S1 and S2). The final PPPI network contained two interconnected clusters (supplemental Figs. S3 and S4), one of which (Cluster 1, supplemental Fig. S3) comprised biological processes classified as: (i) intracellular signal transduction, (ii) ROS metabolism, (iii) small GTPase-mediated signal transduction, (iv) circulatory and blood system processes, and (v) ER stress response (supplemental Tables S3 and S4). PPPI network centrality analysis allows us to assess the importance of a node for a given network, *e.g.* node degree, betweenness, and eigenvector measures (36), expressed as topologic bottleneck data. Centrality analysis of major PDI-associated PPPI network indicated the presence of 50 bottleneck nodes with different scores (Fig. 4), corresponding to ~31% of all nodes present in the PPPI network. Interestingly, the bottlenecks with high score values corresponded to proteins associated with small GTPase signaling processes, NADPH oxidases, intracellular signaling, and PDIA2 (Fig. 4). Given the convergence between PDI and GTPases at central nodes of such networks, we hypothesized that RhoGTPases are a relevant pathway of PDI interaction with NADPH oxidases. This proposal is in line with known characteristics of RhoGTPase signaling such as their recently

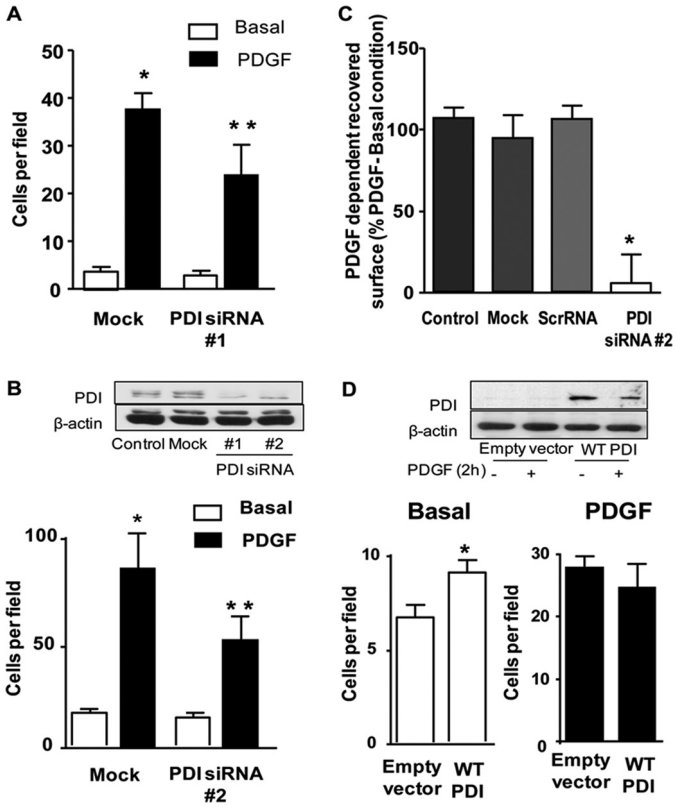

FIGURE 3. **Effects of PDI silencing or overexpression on PDGF-induced VSMC migration.** *A* and *B*, Boyden chamber assay in VSMC transfected with two different siRNA sequence (#1 and #2, see "Experimental Procedures") and exposed or not to PDGF (100 ng/ml; 4 h). Data are expressed as average number of cells/field (4 fields/well). *Inset* shows the effects of PDI siRNA transfection on PDI protein expression. *C*, wound-healing assay in VSMC transfected with PDI siRNA and exposed or not to PDGF (100 ng/ml; 12 h). Data are expressed as difference between the recovered surface after PDGF incubation and base-line condition. *D*, Boyden chamber assay in empty vector-transfected or wild-type (*WT*) PDI-overexpressing VSMC, in conditions similar to *A*. *Inset* shows PDI protein expression after cDNA transfection (Western analysis, with short exposure time). Definitions of specific conditions are described in Fig. 2 legend. Data are mean ± S.D. (*error bars*) of 4 independent experiments per group. *, $p < 0.05$ *versus* basal; **, $p < 0.05$ *versus* control with PDGF.

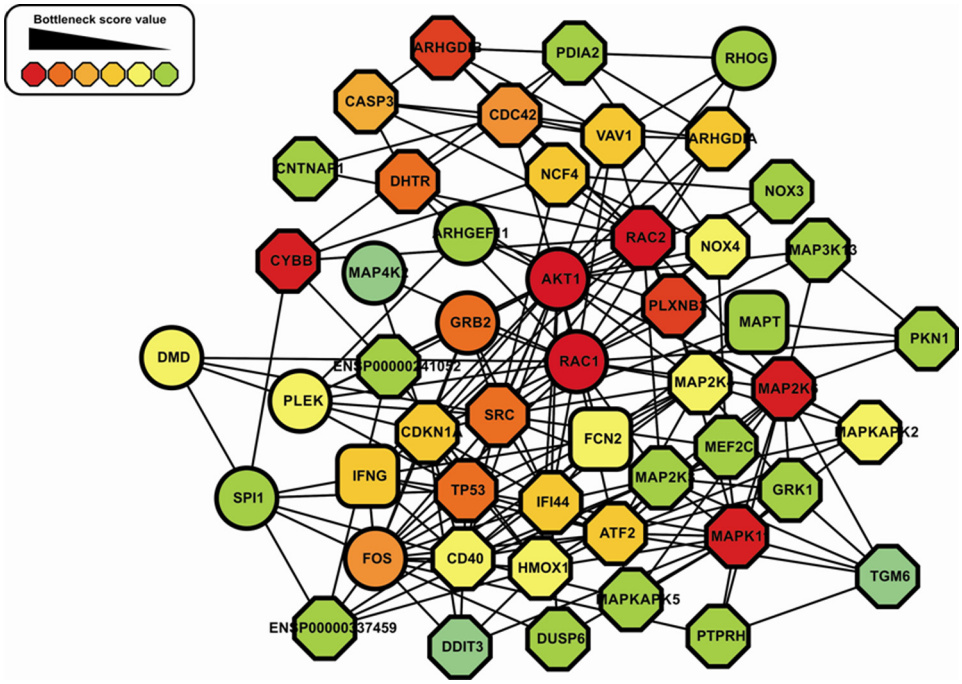

FIGURE 4. **Bottleneck-associated subnetwork obtained from centrality analysis of major PPPI network.** Bottleneck nodes are represent by a *color scale* that indicates its bottleneck score value from highest to lowest value (*inset*). Selected gene names: *ARHGDI*, RhoGDI; *CYBB*, p22^{phox}; *NCF4*, p40^{phox}.

described location at the ER fraction (37), dynamic traffic to membranes, and support of Nox isoforms such as Nox1, Nox2, and Nox3 (38, 39). Importantly, this analysis detected interactions with NADPH oxidase complex subunits that were previously validated by experiments from our group, including catalytic Nox subunits and p47^{phox} (supplemental Fig. S3).

PDGF-induced Rac1 and RhoA Activities Are Decreased by PDI Silencing—To investigate whether PDI is required to support activity of RhoGTPases, we assessed the effects of PDI silencing on basal and PDGF-stimulated activities of Rac1 and RhoA by pulldown assays. Importantly, PDI silencing had negligible effect on base-line GTPase activity compared with scrambled siRNA, but induced pronounced decrease in their total activity after PDGF when compared either with control after PDGF or *versus* base line after PDI silencing (Fig. 5, *A* and *B*). Of note, such changes in activity did not reflect altered protein expression of Rac1, RhoA, and their regulator RhoGDI, as their expression was not significantly altered after exposure to PDGF for distinct time periods in control cells (30 min, 1 h, 4 h, 6 h, and 8 h) (Fig. 5*C*) or by PDI silencing at base line or after PDGF (Fig. 5*D*).

Analysis of PDI Interaction with RhoGTPases and RhoGDI—We further investigated to what extent the functional effects of PDI (an ER lumen-resident enzyme) on RhoGTPases and RhoGDI1 (mainly cytosolic proteins) might reflect some degree of physical interaction, assessed by co-immunoprecipitation analysis. Immunoprecipitation of RhoGDI1, followed by Western blot analysis of PDI showed association between those proteins at base line, which was significantly decreased after PDGF stimulus (10 min and 2 h; Fig. 6*A*). Immunoprecipitation of PDI showed co-immunoprecipitation of either Rac1 or RhoA. Of note, this association was not modulated by exposure to PDGF. This was confirmed by the reverse co-immunoprecipitation with respect to Rac1 (Fig. 6*B*). Again, there was no change in Rac1, RhoA, RhoGDI, or PDI total expression under those conditions (Fig. 6*C*).

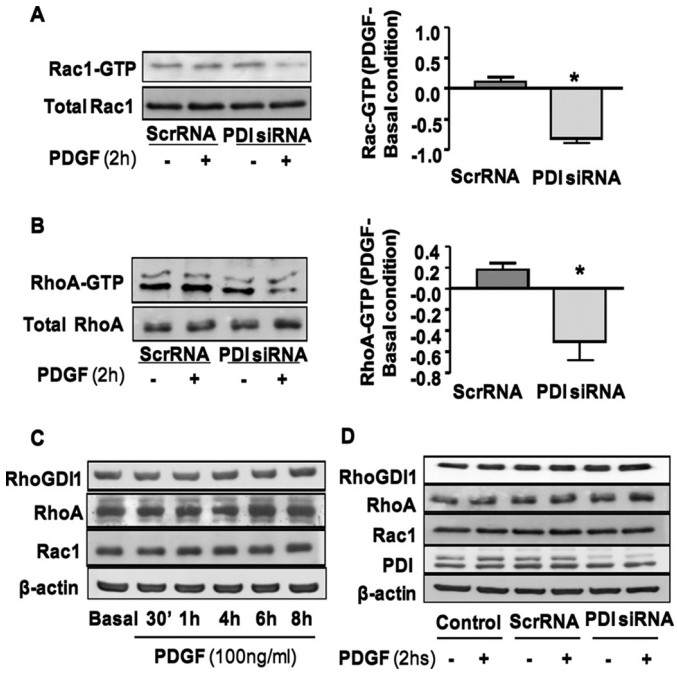

FIGURE 5. **Effects of PDI silencing on PDGF-stimulated activities of Rac1 and RhoA and expression of RhoGTPases and RhoGDI.** RhoGTPase activity was assessed through pulldown assays, as described under "Experimental Procedures." *A*, active Rac1 (*upper*) and total Rac1 (*lower*) and corresponding graph depicting their PDGF-induced quantitative changes in scrambled (*Scr*) or PDI siRNA-transfected VSMC. *B*, similar to *A*, depicting active RhoA (*upper*), total RhoA (*lower*), and quantitative analysis. *C*, Western blot analysis showing expression of RhoGDI and RhoGTPases at distinct times after PDGF incubation. *D*, Western blot analysis showing expression of RhoGDI, RhoGTPases, and PDI in control or PDGF-exposed VSMC. Data are mean ± S.D. (*error bars*) of 3 independent experiments. *, $p < 0.05$ *versus* ScrRNA.

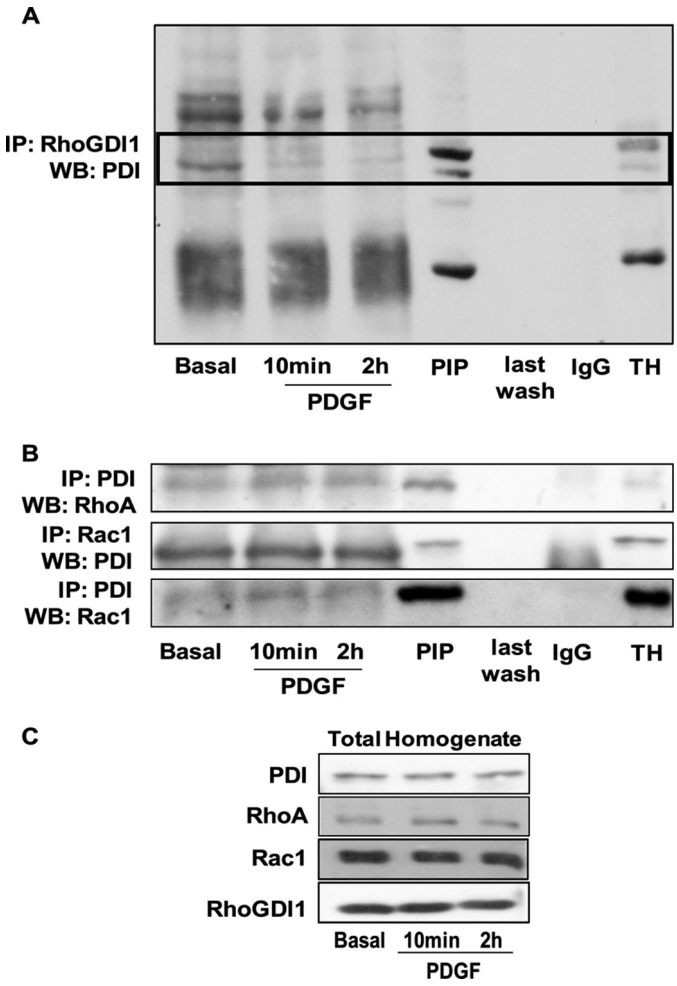

FIGURE 6. **Co-immunoprecipitation between PDI and RhoGDI or RhoGTPases at base line or at PDGF-induced VSMC (10-min or 2-h incubation).** *A*, immunoprecipitation (*IP*) of RhoGDI and Western blot analysis (*WB*) of PDI. *B*, immunoprecipitation of PDI and Western blot analysis of RhoA or Rac1 (*upper* and *lower panel*, respectively). *Middle panel*, immunoprecipitation of Rac1 and Western blot analysis of PDI. *C*, Western blot analysis of total expression of PDI, RhoA, Rac1, and RhoGDI at base line and after PDGF incubation. *PIP*, postimmunoprecipitation supernatant; *last wash*, the last supernatant wash before elution of proteins; *IgG*, 1 μl of the same antibody used for immunoprecipitation, used as Western blot analysis control; *TH*, total homogenate.

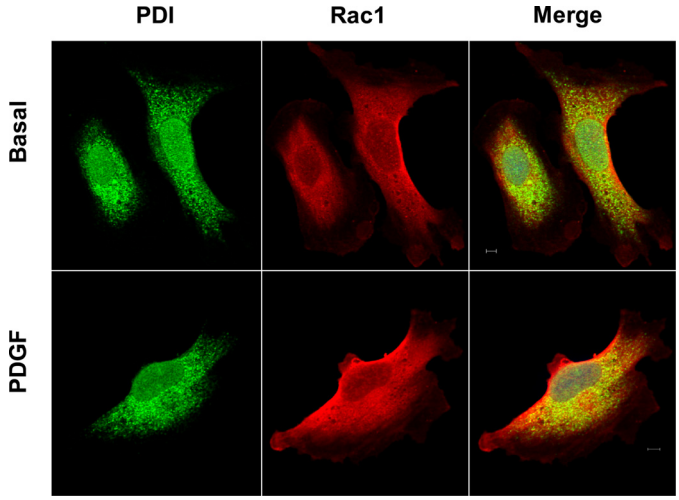

FIGURE 7. **Confocal analysis of PDI and Rac1 expression in the presence or absence of PDGF stimulus.** Immunofluorescence staining of PDI is shown in *green*, Rac1 in *red*, and their merged image in the *right panels*. Confocal microscopy images represent slices of 0.5 μm. *Scale bars*, 5 μm.

To assess subcellular localization of such associations, we performed confocal microscopy analysis, which showed that a minor fraction of Rac1 or RhoGDI pools detectably interact with PDI. There were small though consistently identifiable spots suggestive of co-localization between PDI and Rac1 at the perinuclear region, at base line and after PDGF stimulus (Fig. 7). A similar picture was detected for RhoGDI1 as discrete perinuclear spots at base line, which were decreased after PDGF stimulus (Fig. 8). The antibodies tested against RhoA proved inadequate for immunofluorescence analysis under our conditions.

Effects of PDI Silencing on Adhesion Structures—To assess whether impaired migration and RhoGTPase activation induced disruption of cellular adhesion structures associated with cell motility, we investigated the effect of PDI silencing on focal adhesion and cytoskeletal structures. Confocal analysis of RhoGDI and Rac1 consistently showed their strong staining of circular structures surrounding the peripheral area of the cell, more evident after PDGF stimulation (Fig. 8, *Control*). Concomitant actin staining indicated that: (i) such structures are intracellular; (ii) there was no evidence of F-actin rings, which are the signature of the podosome (40) (Fig. 8). These characteristics, therefore, are more suggestive of recycling vesicular adhesion structures. Importantly, such vesicular structures were decreased in number and size after PDI silencing both at base line and after PDGF stimulus (Fig. 8, siRNA PDI). Furthermore, in PDI-silenced VSMCs, both at base line and after PDGF stimulus, there was a marked decrease in the number of focal adhesions (Fig. 9) and decreased organization of the actin cytoskeleton (Figs. 8 and 9). Together, these findings indicate that PDI silencing induces disruption of cellular adhesion structures and actin cytoskeleton in association with impaired VSMC migration.

DISCUSSION

Our results showed that PDI silencing decreases PDGF-dependent VSMC migration in a context of decreased ROS production, Nox1 mRNA expression and, particularly, reduced activity of Rac1 and RhoA, disruption of adhesion structures and cytoskeletal disorganization. PDI showed association with RhoGDI, decreased after PDGF stimulus, and with Rac and RhoA, unaltered after PDGF incubation. Together, these data indicate an important requirement for PDI in Nox1/redox and RhoGTPase-dependent processes associated with cell migration.

Involvement of ROS derived from either Nox1 (4) or Nox4 (6) in VSMC migration has been shown previously. Substantial loss- or gain-of-function evidence supports the involvement of PDI in functional regulation of distinct NADPH oxidase complexes from VSMCs (8, 10), macrophages (9), or neutrophils (7). In VSMC, we showed convergence between PDI and Nox1, both in response to AngII stimulation (8) or spontaneously upon induced PDI overexpression (8). Functional convergence with Nox4 has not been as clear, although PDI and Nox4 co-localize in VSMC (10), and both Nox4 (41) and PDI silencing[3]

[3] C. X. Santos, J. Wosniak, Jr., M. Terluk, and F. R. M. Laurindo, unpublished observations.

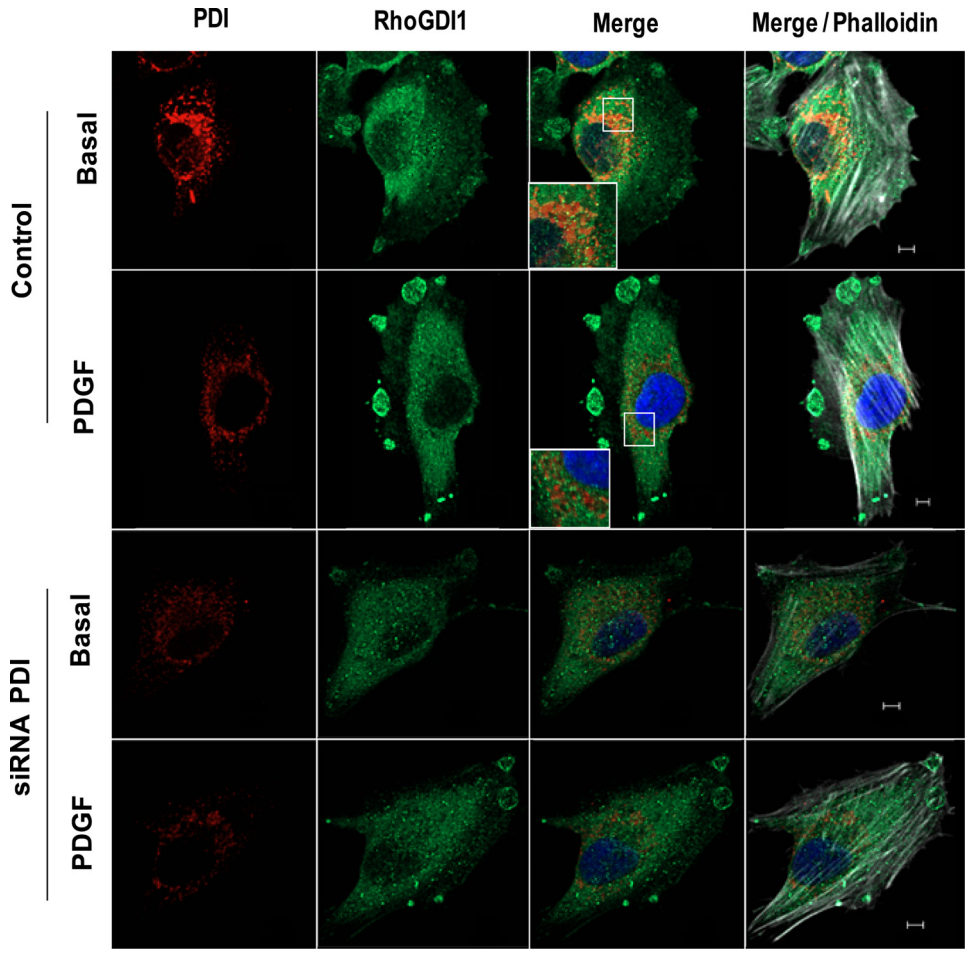

FIGURE 8. **Confocal analysis of PDI and RhoGDI expression in control or PDI-silenced VSMC exposed or not to PDGF.** Immunofluorescence staining of PDI is shown in *red* in *left panels*. Immunostaining for RhoGDI1 is shown in *green*, and their merged images are shown in the absence or not of phalloidin staining (*white*). Nuclei are stained in *blue* (DAPI). Confocal microscopy images represent slices of 0.5 μm. *Scale bars*, 5 μm.

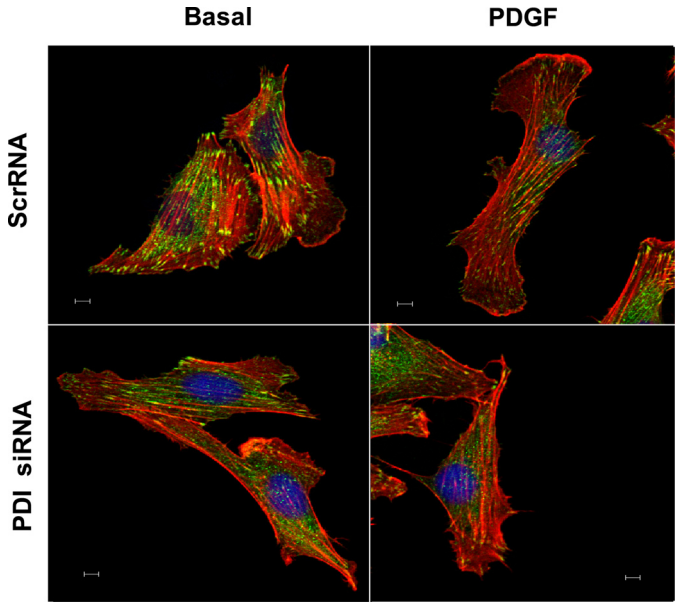

FIGURE 9. **Effects of PDI silencing on focal adhesions.** Confocal microscopic analysis depicts F-actin (phalloidin) in *red* and paxillin staining in *green* in control or PDI-silenced VSMC exposed or not to PDGF. *ScrRNA*, VSMC transfected with scrambled siRNA sequence; *PDI siRNA*, VSMC transfected with siRNA against PDI. *Scale bars*, 5 μm.

decrease ER stress-induced ROS production. The present data support these observations, indicating that another growth factor, namely PDGF, also triggers PDI-dependent Nox1, but not Nox4 expression. Moreover, our data extend the functional implications of these findings by showing that PDI silencing significantly inhibits VSMC migration, assessed through distinct techniques. A crucial question is to what degree the effects of PDI on migration would mainly reflect a nonspecific housekeeping role in protein folding *versus* a more specific Nox-related signaling. Although this is a complex question, there is no evidence suggesting that PDI silencing in our VSMC is associated with toxicity, because cell loss and unfolded protein response markers, including Nox4 induction (8), are not increased in our experimental conditions[3] (41). This agrees with the known cell type-specific sensitivity to PDI knockdown (42). Moreover, evidence for physical interaction between PDI and NADPH oxidase subunits supports some direct regulatory roles of PDI (7–10), in accordance with observed focused effects of PDI silencing in other models (41, 43, 44). The involvement of ER and cytosolic chaperones in signaling processes has been recognized, particularly regarding the assembling of multiprotein complexes (45) or assistance in protein secretion (46). In addition, ER chaperones mediate cell surface processes related to cell adhesion (21, 47–49), coagulation (22),

antigen presentation (18), pathogen invasion (50), and others. Of note, galectin 9-induced T cell migration is abolished by depletion of cell surface PDI (51). These facts suggest that even a protein acting in a central process such as folding can exert specific signaling. VSMC migration is a key event underlying vascular disease such as atherosclerosis and postinjury restenosis. There is evidence for involvement of redox processes in cell migration (24, 52–54), but the underlying mechanisms, particularly regarding Nox-related pathways, are unclear. The involvement of PDI on Nox/ROS-related functional events adds relevant information to understanding the redox control of VSMC migration.

Identifying mechanisms of PDI-Nox interaction is essential to assess the significance of PDI redox effects. Our previous results concentrated on direct interactions between PDI and Nox subunits. Although results showed association with $p22^{phox}$ and catalytic subunits in distinct cell systems (9, 10) and a robust association between PDI and $p47^{phox}$ in the neutrophil cytosol subfraction (7), no clear primary upstream target of PDI emerged, so that a putative PDI effect to assist interaction among multiple complex subunits remained elusive. Because overexpression of either wild-type or cysteine-mutated PDI equally promote spontaneous NADPH oxidase complex activation, at least part of this effect could be due to chaperone PDI effects, known to be thiol-independent (8). The convergence between PDI and GTPases detected in the present work provides novel insights into the upstream mechanisms of PDI-Nox interaction. The use of systems biology PPPI networks to perform unbiased searches for protein interactomes is an evolving strategy to simplify scaffold information to extract theory properties (34). The connections detected for PDI in the available data bases, just as for other signaling proteins such as MAP kinases (55), are more likely to represent protein-protein interactions than client substrates, which interact very transiently with PDI. Indeed, substrate-trapping mutations are needed to pull down specific substrates of PDI family chaperones (56, 57). The observed decrease in PDGF-stimulated Rac1 or RhoA activities in the present work adds a meaningful mechanism whereby PDI affect Nox activity and cell migration. The role of RhoGTPases for Nox1, Nox2, and Nox3 NADPH oxidases is well accepted (38). RhoA activation seems to be a relevant target of Nox4 via Poldip2 regulator (6). However, RhoGTPases also affect nonredox signaling pathways, even when interacting with Nox. Pak1, a known Rac1 target, is phosphorylated in Thr-423 via ROS-dependent PDK1 phosphorylation, but also via nonredox autophosphorylation possibly due to Rac1 (3) Thus, the convergence between PDI and GTPases implies that downstream PDI effects may extend beyond plain Nox/redox regulation.

Although PDI is required to sustain functional activation of Rac1 and RhoA by PDGF, our data suggest that direct PDI-GTPase interaction is unlikely to be responsible *per se* for such effects, given the PDGF-independent co-immunoprecipitation plus small magnitude of their co-localization. On the other hand, it is not unexpected that only a fraction of total pool of cytosolic RhoGTPases will interact with ER-resident PDI; in addition, their interaction could be quite transient. In fact, the majority of the RhoGTPase pool stays inactive in the cytosol, apparently as a reservoir (58). Among possible additional indirect mechanisms mediating PDI interaction with GTPases, the prominence of RhoGDI as a relevant node in our PPPI interactome and its known role in GTPase regulation were noteful. Moreover, RhoGDI binding is necessary, though not sufficient, to support the effects of Rac1 in NADPH oxidase activation in cell-free neutrophil system (59) or cardiomyocytes (60), and RhoGDI silencing affects cell migration (37, 61). Together with these considerations, co-immunoprecipitation of PDI with RhoGDI at base line and its absence after PDGF activation in the present work are consistent with a dynamic role of RhoGDI in the regulation of PDI convergence with GTPase and Nox activation. Here, two issues can be discussed.

First, the association between ER *versus* cytosolic-located proteins is not surprising: previous examples in the ER fraction indicated interaction between PDI with native SOD1 (62), Grp58 with TORC1 (63), and Rac1 with TORC2 (64), the last reportedly an ER protein (65). Furthermore, Rac1 and RhoA are reportedly detected in the ER-containing fraction and co-fractionate with PDI (37). Alternatively, a fraction of PDI may reach the cell periphery either via ER-related extensions or vesicles (66) or via yet unknown mechanisms allowing escape from ER retrieval (35).

Second, the mechanisms of GDI effects may be complex: in addition to the classical role of extracting active RhoGTPases from membranes (37), RhoGDI binding to GTPases was recently shown to protect them from proteasome degradation and to support their delivery to membranes (37). Indeed, the GDP-bound GDI complex can support NADPH oxidase activation to an extent not dissimilar from that of GTP-bound Rac (59). In addition, there is increasing evidence for a slow alternative RhoGDI-independent GTPase delivery to membranes by vesicle trafficking (67). Further evidence for complexity of GTPase regulation is given by unexpectedly increased Rac1 activation in geranylgeranyl-transferase-deficient mice (68). Therefore, the net effect of RhoGDI on overall RhoGTPase regulation depends on multiple factors, including cell type. Whereas in fast-migrating melanoma cells, RhoGDI1 knockdown decreases migration and its persistence (37), slowly migrating bladder cancer cells increase their migration upon RhoGDI1 silencing (61). We hypothesize that our VSMC exposed to PDGF behave similarly to fast-migrating cancer cells, in which GDI-mediated delivery of RhoGTPases to membranes predominates over its other actions. In this context, the interaction with PDI could help to assist or prime the GDI-GTPase complex to growth factor activation. In plants, RhoGDI accounts for polar organization of GTPase activation, oxidant generation, and root hair growth (69, 70). In our VSMCs, the loss of organized directional migration due to PDI silencing and simultaneous loss of both Rac1 and RhoA activation is consistent with a RhoGDI-related delivery defect regarding Rac1/RhoA.

In summary, our data indicate a requirement for the ER redox chaperone PDI in redox/Nox1 and GTPase-dependent VSMC migration. This pathway adds a novel regulatory level to this disease-relevant cellular process and provides physiological dimension to PDI-NADPH oxidase interaction. The observed convergence among PDI and Rac1/RhoA activation,

RhoGDI binding, and cytoskeletal organization reinforces a possible role of PDI as NADPH oxidase organizer, already suggested concerning the mode of PDI interaction with $p47^{phox}$ in neutrophils (7).

Acknowledgments—We thank Guy Capriolo for manufacturing the Boyden chamber, Ana L. Garippo and Maria Bertoline for technical support, and Denise C. Fernandes for helpful discussion.

REFERENCES

1. Schwartz, S. M. (1997) Perspectives series. Cell adhesion in vascular biology: smooth muscle migration in atherosclerosis and restenosis. *J. Clin. Invest.* **99,** 2814–2816
2. Sundaresan, M., Yu, Z. X., Ferrans, V. J., Irani, K., and Finkel, T. (1995) Requirement for generation of H_2O_2 for platelet-derived growth factor signal transduction. *Science* **270,** 296–299
3. Weber, D. S., Taniyama, Y., Rocic, P., Seshiah, P. N., Dechert, M. A., Gerthoffer, W. T., and Griendling, K. K. (2004) Phosphoinositide-dependent kinase 1 and p21-activated protein kinase mediate reactive oxygen species-dependent regulation of platelet-derived growth factor-induced smooth muscle cell migration. *Circ. Res.* **94,** 1219–1226
4. Schröder, K., Helmcke, I., Palfi, K., Krause, K. H., Busse, R., and Brandes, R. P. (2007) Nox1 mediates basic fibroblast growth factor-induced migration of vascular smooth muscle cells. *Arterioscler. Thromb. Vasc. Biol.* **27,** 1736–1743
5. Zimmerman, M. C., Takapoo, M., Jagadeesha, D. K., Stanic, B., Banfi, B., Bhalla, R. C., and Miller, F. J., Jr. (2011) Activation of NADPH oxidase 1 increases intracellular calcium and migration of smooth muscle cells. *Hypertension* **58,** 446–453
6. Lyle, A. N., Deshpande, N. N., Taniyama, Y., Seidel-Rogol, B., Pounkova, L., Du, P., Papaharalambus, C., Lassègue, B., and Griendling, K. K. (2009) Poldip2, a novel regulator of Nox4 and cytoskeletal integrity in vascular smooth muscle cells. *Circ. Res.* **105,** 249–259
7. de A Paes, A. M., Veríssimo-Filho, S., Guimarães, L. L., Silva, A. C., Takiuti, J. T., Santos, C. X., Janiszewski, M., Laurindo, F. R., and Lopes, L. R. (2011) Protein disulfide isomerase redox-dependent association with $p47^{phox}$: evidence for an organizer role in leukocyte NADPH oxidase activation. *J. Leukoc. Biol.* **90,** 799–810
8. Fernandes, D. C., Manoel, A. H., Wosniak, J., Jr., and Laurindo, F. R. (2009) Protein disulfide isomerase overexpression in vascular smooth muscle cells induces spontaneous preemptive NADPH oxidase activation and Nox1 mRNA expression: effects of nitrosothiol exposure. *Arch. Biochem. Biophys.* **484,** 197–204
9. Santos, C. X., Stolf, B. S., Takemoto, P. V., Amanso, A. M., Lopes, L. R., Souza, E. B., Goto, H., and Laurindo, F. R. (2009) Protein disulfide isomerase (PDI) associates with NADPH oxidase and is required for phagocytosis of *Leishmania chagasi* promastigotes by macrophages. *J. Leukoc. Biol.* **86,** 989–998
10. Janiszewski, M., Lopes, L. R., Carmo, A. O., Pedro, M. A., Brandes, R. P., Santos, C. X., and Laurindo, F. R. (2005) Regulation of NAD(P)H oxidase by associated protein disulfide isomerase in vascular smooth muscle cells. *J. Biol. Chem.* **280,** 40813–40819
11. Clissold, P. M., and Bicknell, R. (2003) The thioredoxin-like fold: hidden domains in protein disulfide isomerases and other chaperone proteins. *Bioessays* **25,** 603–611
12. Ellgaard, L., and Ruddock, L. W. (2005) The human protein disulphide isomerase family: substrate interactions and functional properties. *EMBO Rep.* **6,** 28–32
13. Noiva, R. (1999) Protein disulfide isomerase: the multifunctional redox chaperone of the endoplasmic reticulum. *Semin. Cell Dev. Biol.* **10,** 481–493
14. Wilkinson, B., and Gilbert, H. F. (2004) Protein disulfide isomerase. *Biochim. Biophys. Acta* **1699,** 35–44
15. Gruber, C. W., Cemazar, M., Heras, B., Martin, J. L., and Craik, D. J. (2006) Protein disulfide isomerase: the structure of oxidative folding. *Trends Biochem. Sci.* **31,** 455–464
16. Keller, M., Rüegg, A., Werner, S., and Beer, H. D. (2008) Active caspase-1 is a regulator of unconventional protein secretion. *Cell* **132,** 818–831
17. Haefliger, S., Klebig, C., Schaubitzer, K., Schardt, J., Timchenko, N., Mueller, B. U., and Pabst, T. (2011) Protein disulfide isomerase blocks CEBPA translation and is up-regulated during the unfolded protein response in AML. *Blood* **117,** 5931–5940
18. Park, B., Lee, S., Kim, E., Cho, K., Riddell, S. R., Cho, S., and Ahn, K. (2006) Redox regulation facilitates optimal peptide selection by MHC class I during antigen processing. *Cell* **127,** 369–382
19. Faé, K. C., Diefenbach da Silva, D., Bilate, A. M., Tanaka, A. C., Pomerantzeff, P. M., Kiss, M. H., Silva, C. A., Cunha-Neto, E., Kalil, J., and Guilherme, L. (2008) PDIA3, HSPA5 and vimentin, proteins identified by 2-DE in the valvular tissue, are the target antigens of peripheral and heart infiltrating T cells from chronic rheumatic heart disease patients. *J. Autoimmun.* **31,** 136–141
20. Terada, K., Manchikalapudi, P., Noiva, R., Jauregui, H. O., Stockert, R. J., and Schilsky, M. L. (1995) Secretion, surface localization, turnover, and steady state expression of protein disulfide isomerase in rat hepatocytes. *J. Biol. Chem.* **270,** 20410–20416
21. Essex, D. W., Li, M., Miller, A., and Feinman, R. D. (2001) Protein disulfide isomerase and sulfhydryl-dependent pathways in platelet activation. *Biochemistry* **40,** 6070–6075
22. Ahamed, J., Versteeg, H. H., Kerver, M., Chen, V. M., Mueller, B. M., Hogg, P. J., and Ruf, W. (2006) Disulfide isomerization switches tissue factor from coagulation to cell signaling. *Proc. Natl. Acad. Sci. U.S.A.* **103,** 13932–13937
23. Laurindo, F. R., de Souza, H. P., Pedro Mde, A., and Janiszewski, M. (2002) Redox aspects of vascular response to injury. *Methods Enzymol.* **352,** 432–454
24. Fernandes, D. C., Wosniak, J., Jr., Pescatore, L. A., Bertoline, M. A., Liberman, M., Laurindo, F. R., and Santos, C. X. (2007) Analysis of DHE-derived oxidation products by HPLC in the assessment of superoxide production and NADPH oxidase activity in vascular systems. *Am. J. Physiol. Cell Physiol.* **292,** C413–422
25. Taboubi, S., Milanini, J., Delamarre, E., Parat, F., Garrouste, F., Pommier, G., Takasaki, J., Hubaud, J. C., Kovacic, H., and Lehmann, M. (2007) G alpha(q/11)-coupled P2Y2 nucleotide receptor inhibits human keratinocyte spreading and migration. *FASEB J.* **21,** 4047–4058
26. Wosniak, J., Jr., Santos, C. X., Kowaltowski, A. J., and Laurindo, F. R. (2009) Cross-talk between mitochondria and NADPH oxidase: effects of mild mitochondrial dysfunction on angiotensin II-mediated increase in Nox isoform expression and activity in vascular smooth muscle cells. *Antioxid. Redox Signal.* **11,** 1265–1278
27. Ren, X. D., Kiosses, W. B., and Schwartz, M. A. (1999) Regulation of the small GTP-binding protein Rho by cell adhesion and the cytoskeleton. *EMBO J.* **18,** 578–585
28. Shannon, P., Markiel, A., Ozier, O., Baliga, N. S., Wang, J. T., Ramage, D., Amin, N., Schwikowski, B., and Ideker, T. (2003) Cytoscape: a software environment for integrated models of biomolecular interaction networks. *Genome Res.* **13,** 2498–2504
29. Bader, G. D., and Hogue, C. W. (2003) An automated method for finding molecular complexes in large protein interaction networks. *BMC Bioinformatics* **4,** 2
30. Lin, C. Y., Chin, C. H., Wu, H. H., Chen, S. H., Ho, C. W., and Ko, M. T. (2008) Hubba: hub objects analyzer, a framework of interactome hubs identification for network biology. *Nucleic Acids Res.* **36,** W438–443
31. Maere, S., Heymans, K., and Kuiper, M. (2005) BiNGO: a Cytoscape plugin to assess overrepresentation of gene ontology categories in biological networks. *Bioinformatics* **21,** 3448–3449
32. Rivals, I., Personnaz, L., Taing, L., and Potier, M. C. (2007) Enrichment or depletion of a GO category within a class of genes: which test? *Bioinformatics* **23,** 401–407
33. Benjamini, Y., and Hochberg, Y. (1995) Controlling the false discovery rate: a practical and powerful approach to multiple testing. *J. Royal Statistical Society Series B-Methodological* **57,** 289–300
34. Vidal, M., Cusick, M. E., and Barabási, A. L. (2011) Interactome networks and human disease. *Cell* **144,** 986–998

35. Hatahet, F., and Ruddock, L. W. (2009) Protein disulfide isomerase: a critical evaluation of its function in disulfide bond formation. *Antioxid. Redox Signal.* **11,** 2807–2850
36. Borgatti, S. P. (2005) Centrality and network flow. *Social Networks* **27,** 55–71
37. Boulter, E., Garcia-Mata, R., Guilluy, C., Dubash, A., Rossi, G., Brennwald, P. J., and Burridge, K. (2010) Regulation of RhoGTPase cross-talk, degradation and activity by RhoGDI1. *Nat. Cell Biol.* **12,** 477–483
38. Hordijk, P. L. (2006) Regulation of NADPH oxidases: the role of Rac proteins. *Circ. Res.* **98,** 453–462
39. Brown, D. I., and Griendling, K. K. (2009) Nox proteins in signal transduction. *Free Radic. Biol. Med.* **47,** 1239–1253
40. Linder, S., and Aepfelbacher, M. (2003) Podosomes: adhesion hot-spots of invasive cells. *Trends Cell Biol.* **13,** 376–385
41. Santos, C. X., Tanaka, L. Y., Wosniak, J., and Laurindo, F. R. (2009) Mechanisms and implications of reactive oxygen species generation during the unfolded protein response: roles of endoplasmic reticulum oxidoreductases, mitochondrial electron transport, and NADPH oxidase. *Antioxid. Redox Signal.* **11,** 2409–2427
42. Hashida, T., Kotake, Y., and Ohta, S. (2011) Protein disulfide isomerase knockdown-induced cell death is cell line-dependent and involves apoptosis in MCF-7 cells. *J. Toxicol. Sci.* **36,** 1–7
43. Maruri-Avidal, L., López, S., and Arias, C. F. (2008) Endoplasmic reticulum chaperones are involved in the morphogenesis of rotavirus infectious particles. *J. Virol.* **82,** 5368–5380
44. Zhou, M., Jacob, A., Ho, N., Miksa, M., Wu, R., Maitra, S. R., and Wang, P. (2008) Down-regulation of protein disulfide isomerase in sepsis and its role in tumor necrosis factor-α release. *Crit. Care* **12,** R100
45. Christis, C., Lubsen, N. H., and Braakman, I. (2008) Protein folding includes oligomerization: examples from the endoplasmic reticulum and cytosol. *FEBS J.* **275,** 4700–4727
46. Delom, F., Mallet, B., Carayon, P., and Lejeune, P. J. (2001) Role of extracellular molecular chaperones in the folding of oxidized proteins: refolding of colloidal thyroglobulin by protein disulfide isomerase and immunoglobulin heavy chain-binding protein. *J. Biol. Chem.* **276,** 21337–21342
47. Lahav, J., Jurk, K., Hess, O., Barnes, M. J., Farndale, R. W., Luboshitz, J., and Kehrel, B. E. (2002) Sustained integrin ligation involves extracellular free sulfhydryls and enzymatically catalyzed disulfide exchange. *Blood* **100,** 2472–2478
48. Lahav, J., Gofer-Dadosh, N., Luboshitz, J., Hess, O., and Shaklai, M. (2000) Protein disulfide isomerase mediates integrin-dependent adhesion. *FEBS Lett.* **475,** 89–92
49. Essex, D. W., Chen, K., and Swiatkowska, M. (1995) Localization of protein disulfide isomerase to the external surface of the platelet plasma membrane. *Blood* **86,** 2168–2173
50. Gallina, A., Hanley, T. M., Mandel, R., Trahey, M., Broder, C. C., Viglianti, G. A., and Ryser, H. J. (2002) Inhibitors of protein-disulfide isomerase prevent cleavage of disulfide bonds in receptor-bound glycoprotein 120 and prevent HIV-1 entry. *J. Biol. Chem.* **277,** 50579–50588
51. Bi, S., Hong, P. W., Lee, B., and Baum, L. G. (2011) Galectin-9 binding to cell surface protein disulfide isomerase regulates the redox environment to enhance T-cell migration and HIV entry. *Proc. Natl. Acad. Sci. U.S.A.* **108,** 10650–10655
52. Souza, H. P., Souza, L. C., Anastacio, V. M., Pereira, A. C., Junqueira, M. L., Krieger, J. E., da Luz, P. L., Augusto, O., and Laurindo, F. R. (2000) Vascular oxidant stress early after balloon injury: evidence for increased NAD(P)H oxidoreductase activity. *Free Radic. Biol. Med.* **28,** 1232–1242
53. Azevedo, L. C., Pedro, M. A., Souza, L. C., de Souza, H. P., Janiszewski, M., da Luz, P. L., and Laurindo, F. R. (2000) Oxidative stress as a signaling mechanism of the vascular response to injury: the redox hypothesis of restenosis. *Cardiovasc. Res.* **47,** 436–445
54. Leite, P. F., Danilovic, A., Moriel, P., Dantas, K., Marklund, S., Dantas, A. P., and Laurindo, F. R. (2003) Sustained decrease in superoxide dismutase activity underlies constrictive remodeling after balloon injury in rabbits. *Arterioscler. Thromb. Vasc. Biol.* **23,** 2197–2202
55. Bandyopadhyay, S., Chiang, C. Y., Srivastava, J., Gersten, M., White, S., Bell, R., Kurschner, C., Martin, C. H., Smoot, M., Sahasrabudhe, S., Barber, D. L., Chanda, S. K., and Ideker, T. (2010) A human MAP kinase interactome. *Nat. Methods* **7,** 801–805
56. Zito, E., Melo, E. P., Yang, Y., Wahlander, Å., Neubert, T. A., and Ron, D. (2010) Oxidative protein folding by an endoplasmic reticulum-localized peroxiredoxin. *Mol. Cell* **40,** 787–797
57. Jessop, C. E., Watkins, R. H., Simmons, J. J., Tasab, M., and Bulleid, N. J. (2009) Protein disulphide isomerase family members show distinct substrate specificity: P5 is targeted to BiP client proteins. *J. Cell Sci.* **122,** 4287–4295
58. Garcia-Mata, R., Boulter, E., and Burridge, K. (2011) The "invisible hand": regulation of RhoGTPases by RHOGDIs. *Nat. Rev. Mol. Cell Biol.* **12,** 493–504
59. Di-Poï, N., Fauré, J., Grizot, S., Molnár, G., Pick, E., and Dagher, M. C. (2001) Mechanism of NADPH oxidase activation by the Rac/Rho-GDI complex. *Biochemistry* **40,** 10014–10022
60. Custodis, F., Eberl, M., Kilter, H., Böhm, M., and Laufs, U. (2006) Association of RhoGDIα with Rac1 GTPase mediates free radical production during myocardial hypertrophy. *Cardiovasc. Res.* **71,** 342–351
61. Moissoglu, K., McRoberts, K. S., Meier, J. A., Theodorescu, D., and Schwartz, M. A. (2009) RhoGDP dissociation inhibitor 2 suppresses metastasis via unconventional regulation of RhoGTPases. *Cancer Res.* **69,** 2838–2844
62. Atkin, J. D., Farg, M. A., Turner, B. J., Tomas, D., Lysaght, J. A., Nunan, J., Rembach, A., Nagley, P., Beart, P. M., Cheema, S. S., and Horne, M. K. (2006) Induction of the unfolded protein response in familial amyotrophic lateral sclerosis and association of protein-disulfide isomerase with superoxide dismutase 1. *J. Biol. Chem.* **281,** 30152–30165
63. Ramírez-Rangel, I., Bracho-Valdés, I., Vázquez-Macías, A., Carretero-Ortega, J., Reyes-Cruz, G., and Vázquez-Prado, J. (2011) Regulation of mTORC1 complex assembly and signaling by GRp58/ERp57. *Mol. Cell. Biol.* **31,** 1657–1671
64. Saci, A., Cantley, L. C., and Carpenter, C. L. (2011) Rac1 regulates the activity of mTORC1 and mTORC2 and controls cellular size. *Mol. Cell* **42,** 50–61
65. Boulbés, D. R., Shaiken, T., and Sarbassov dos, D. (2011) Endoplasmic reticulum is a main localization site of mTORC2. *Biochem. Biophys. Res. Commun.* **413,** 46–52
66. Spang, A. (2009) On vesicle formation and tethering in the ER-Golgi shuttle. *Curr. Opin. Cell Biol.* **21,** 531–536
67. Slaughter, B. D., Das, A., Schwartz, J. W., Rubinstein, B., and Li, R. (2009) Dual modes of cdc42 recycling fine-tune polarized morphogenesis. *Dev. Cell* **17,** 823–835
68. Khan, O. M., Ibrahim, M. X., Jonsson, I. M., Karlsson, C., Liu, M., Sjogren, A. K., Olofsson, F. J., Brisslert, M., Andersson, S., Ohlsson, C., Hultén, L. M., Bokarewa, M., and Bergo, M. O. (2011) Geranylgeranyltransferase type I (GGTase-I) deficiency hyperactivates macrophages and induces erosive arthritis in mice. *J. Clin. Invest.* **121,** 628–639
69. Carol, R. J., Takeda, S., Linstead, P., Durrant, M. C., Kakesova, H., Derbyshire, P., Drea, S., Zarsky, V., and Dolan, L. (2005) A RhoGDP dissociation inhibitor spatially regulates growth in root hair cells. *Nature* **438,** 1013–1016
70. Kost, B. (2008) Spatial control of Rho (Rac-Rop) signaling in tip-growing plant cells. *Trends Cell Biol.* **18,** 119–127